

# Particle-laden flow down a slope in uniform stratification

Kate Snow<sup>1,2</sup> and B. R. Sutherland<sup>3,†</sup>

<sup>1</sup>Research School of Earth Sciences, Australian National University, Acton, ACT 0200, Australia

<sup>2</sup>ARC Centre of Excellence for Climate System Science, University of New South Wales, Sydney, NSW 2052, Australia

<sup>3</sup>Department of Physics, University of Alberta, Edmonton, T6G 2E1, Canada

(Received 18 March 2014; revised 14 July 2014; accepted 15 July 2014)

Lock–release laboratory experiments are performed to examine saline and particle-laden flows down a slope into both constant-density and linearly stratified ambients. Both hypopycnal (surface-propagating) currents and hyperpycnal (turbidity) currents are examined, with the focus being upon the influence of ambient stratification on turbidity currents. Measurements are made of the along-slope front speed and the depth at which the turbidity current separates from the slope and intrudes into the ambient. These results are compared to the predictions of a theory that characterizes the flow evolution and separation depth in terms of the slope  $s$ , the entrainment parameter  $E$  (the ratio of entrainment to flow speed), the relative stratification parameter  $S$  (the ratio of the ambient density difference to the relative current density) and a new parameter  $\gamma$  defined to be the ratio of the particle settling to entrainment speed. The implicit prediction for the separation depth,  $H_s$ , is made explicit by considering limits of small and large separation depth. In the former case of a ‘weak’ turbidity current, entrainment and particle settling are unimportant and separation occurs where the density of the ambient fluid equals the density of the fluid in the lock. In the latter case of a ‘strong’ turbidity current, entrainment and particle settling crucially affect the separation depth. Consistent with theory, we find that the separation depth indeed depends on  $\gamma$  if the particle size (and hence settling rate) is sufficiently large and if the current propagates many lock lengths before separating from the slope. A composite prediction that combines the explicit formulae for the separation depth for weak and strong turbidity currents agrees well with experimental measurements over a wide parameter range.

**Key words:** geophysical and geological flows, multiphase and particle-laden flows, stratified flows

## 1. Introduction

Particle-bearing flows are said to be ‘hypopycnal’ (or an ‘overflow’) if the combined density of the sediment and interstitial fluid is lower than that of the ambient, which is assumed to be particle-free. If the combined density is higher than that of the ambient, it is said to be ‘hyperpycnal’ (or an ‘underflow’). If the density

† Email address for correspondence: [bruce.sutherland@ualberta.ca](mailto:bruce.sutherland@ualberta.ca)

due to particles primarily controls the buoyancy of the current, such particle-laden bottom-propagating flows are more generally called turbidity currents. Understanding the evolution of turbidity currents is of paramount importance in consideration of marine construction and infrastructure near river mouths (Mulder & Syvitski 1995; Mulder *et al.* 2003) and on continental shelves (Bruschi *et al.* 2006; Lawrence, McCaffrey & Talling 2009). These currents occur in many different circumstances in nature, for example, at the outflow of rivers into the ocean (Mulder & Syvitski 1995; Mulder *et al.* 2003), where they may be generated by storm waves impacting the coast (Shepard *et al.* 2013), in regions of submarine landslides resulting for example from tectonic activity (Masson *et al.* 2011) and where tidal activity acts on steep slopes (Thomson *et al.* 2010). Though many idealized studies have examined turbidity currents in uniform-density ambient fluids, their evolution in a stratified fluid is poorly understood. Here, through both laboratory experiments and scaling theory, we provide insight into the speed and boundary separation of turbidity currents in circumstances where both slope and stratification play a key role.

Only limited observational records exist for the occurrence and flow of turbidity currents. This is due to the difficulty in predicting the time and frequency of turbidity currents as well as the destructive nature of such sediment-laden flows (Paull *et al.* 2003; Straub 2007). Owing to the lack of observations and ongoing challenges in numerical modelling of particle-laden flows, experimental and theoretical methods are best employed to gain an increased understanding of the evolution of turbidity currents.

Most studies of particle-driven flows have considered a flat-bottom set-up with a constant-density ambient (Bonnecaze, Huppert & Lister 1993; Sparks *et al.* 1993; Hurzeler, Ivey & Imberger 1995; Hogg, Huppert & Hallworth 1999, 2000). Through experiments and theory, Bonnecaze & Lister (1999) examined particle-laden currents on sloping bottoms in uniform-density ambients. They developed a scaling analysis for such currents, incorporating both entrainment and frictional effects. From this, they determined the deposition of particles from turbidity currents as it depends upon entrainment.

Turbidity currents down a sloping bottom were also investigated in some of the experiments of Parson, Bush & Syvitski (2001). Their investigation of particle-bearing hypopycnal plumes in a uniform-density ambient examined circumstances whereby convective instabilities associated with settling particles produced a hyperpycnal plume that ran down the sloping bottom. They found that the production of such a hyperpycnal plume occurred if the sediment concentration exceeded  $5 \text{ kg m}^{-3}$ .

The effects of ambient stratification upon propagating particle-laden currents was investigated through lock–release experiments of intrusive particle-laden and saline currents entering a two-layer stratification (Rimoldi, Alexander & Morris 1996; de Rooij, Linden & Dalziel 1999) and a continuous stratification (de Rooij 1999). The latter study showed that particle-laden intrusions propagating within the stratified ambient (sometimes called an ‘interflow’) initially evolve in a similar fashion to saline intrusions. However, the settling of particles eventually leads to the intrusion separating into two currents, one composed primarily of the light interstitial fluid that rises to become a hypopycnal surface flow and one composed of high-particle concentrations advancing as a bottom flow. They applied a simple scaling model to determine the distance at which the intrusion split into two boundary currents and found the length to be dependent on the settling speed of the particles.

A different avenue of research has examined the effect of bottom topographic slope upon the evolution of particle-free saline gravity currents. In particular, laboratory experiments (Britter & Linden 1980) and numerical simulations (Birman *et al.* 2007; Tokyay & Garcia 2014) have shown that slope has little effect on the front speed in a uniform-density ambient. While a larger slope allowed for increased gravitational force on the current, it also led to increased entrainment, which decreased the current's momentum. Together, the two forces counteracted any increase or decrease in speed as slope was varied (Britter & Linden 1980; Beghin, Hopfinger & Britter 1981).

In a uniformly stratified fluid, slope is used to characterize the dense flow as an entraining plume or a detraining gravity current and acts to define where the flow separates from the bottom and intrudes into the ambient at its neutral buoyancy level (Baines 2001, 2008; Wells & Nadarajah 2009). The intrusion can then go on to excite internal waves ahead of the gravity current (Monaghan *et al.* 1999).

To attain a more complete understanding of the characteristics of turbidity currents entering the ocean and thermally stratified lakes (de Cesare, Boillat & Schleiss 2006), the effects of both stratification and slope must be taken into account. Yet no studies have previously been undertaken to examine these combined effects upon particle-laden flows. As well as helping in the management of pollutant transports and the understanding of nutrient transport by turbidity flows entering the ocean (Chung & Gu 1998) and stratified lakes (Cortés *et al.* 2014), such a study could help assess the suitability and tolerance of subaqueous structures constructed by the oil industry near river mouths and on continental shelves. In developing such an assessment, it is not the sediment deposition itself that is key. Rather, the most useful information is the depth at which the turbidity current separates from the ocean or stratified lake (Antenucci *et al.* 2005) floor and intrudes into the stratified ambient. This separation depth delimits where the turbidity current stops acting destructively along the ocean or lake bottom. For these reasons, our study focuses upon developing a prediction, tested by laboratory experiments, for the depth at which the intrusion occurs as it depends upon particle size and concentration, topographic slope and ambient stratification.

In §2, scaling theory and existing empirical models are adapted to formulate predictions for the speed and separation depth of turbidity currents in a stratified ambient. The set-up of the lock–release laboratory experiments designed to test the predictions is outlined in §3. In §4 we present qualitative results comparing the evolution of saline and particle-bearing flows and the evolution of turbidity currents in stratified and uniform-density ambients. There we also show how a hypopycnal flow can create a hyperpycnal flow and vice versa. Quantitative results comparing the predictions of flow speed and separation depth to turbidity current experiments is presented in §5. The results are summarized in §6.

## 2. Theory

Here we adapt existing theories to formulate expressions for the speed and separation depth of a particle-laden current flowing down a slope  $s$  in a uniformly stratified fluid. We first review theories for the speed of gravity currents propagating along a horizontal bottom within uniform-density or uniformly stratified ambients. We then adapt a box-model approach to predict the evolution of interstitial density and particle concentration in a turbidity current. The resulting prediction of the composite current density as a function of along-slope distance is used to predict the separation depth for a downslope current in a uniformly stratified ambient.

### 2.1. Current speed

Here we model the steady speed,  $U$ , of a high-Reynolds-number gravity current released from a full-depth lock of height  $h_0$  moving over a flat bottom.

For an ambient of uniform density,  $\rho_0$ , the speed of a gravity current of density  $\rho_{c0}$  is

$$U = Fr_0 \sqrt{g'_0 h_0}, \quad (2.1)$$

in which  $Fr_0$  is the Froude number and

$$g'_0 \equiv g \frac{\rho_{c0} - \rho_0}{\rho_0} \quad (2.2)$$

is the reduced gravity based on the relative lock fluid density, with  $g$  the gravitational constant. For energy-conserving currents, the Froude number based on the lock height is predicted to be  $Fr_0 = 1/2$  (Benjamin 1968), moderately larger than the value, 0.48, measured in laboratory experiments (Shin, Dalziel & Linden 2004).

Next we consider a current propagating beneath a uniformly stratified ambient whose density increases linearly from  $\rho_T$  at the top to  $\rho_B$  at its deepest point. The corresponding (constant) squared buoyancy frequency in the Boussinesq approximation is defined by

$$N^2 = -\frac{g}{\rho_0} \frac{d\bar{\rho}}{dz} = g \frac{\rho_B - \rho_T}{\rho_T H}, \quad (2.3)$$

where  $H$  is the depth of the fluid at its deepest point and the reference density  $\rho_0$  may arbitrarily be taken to equal the surface density,  $\rho_T$ .

If the density of the lock fluid matches the density  $\rho_{h0}$  of the ambient outside the bottom of the lock at depth  $h_0$  (where  $h_0 = H$  and  $\rho_{h0} = \rho_B$  if the bottom is horizontal), the resulting gravity current speed is

$$U = Fr_1 N h_0, \quad (2.4)$$

in which the Froude number is predicted to be  $Fr_1 = 1/4$  (Ungarish 2006), consistent with experimental measurements of 0.266 (Maxworthy *et al.* 2002).

In general, if the lock fluid density is larger than the ambient density outside the bottom of the lock, we can write the speed in terms of a Froude number  $Fr_S$  through

$$U = Fr_S \sqrt{g'_0 h_0}, \quad (2.5)$$

where  $g'_0$  is given by (2.2) and  $Fr_S$  varies with the relative magnitude of the stratification,  $S$ . This parameter was introduced by Ungarish (2006) in his study of gravity currents propagating along a flat bottom underneath a linearly stratified ambient. Explicitly,

$$S \equiv \frac{\rho_{h0} - \rho_0}{\rho_{c0} - \rho_0} = \left( \frac{N h_0}{\sqrt{g'_0 h_0}} \right)^2, \quad (2.6)$$

in which  $\rho_0 = \rho_T$  is the ambient density at the top of the fluid. If the ambient is weakly stratified ( $S \ll 1$ ), Ungarish (2006) predicted  $Fr_S \simeq Fr_0 (1 - 2S/3)^{1/2}$ , in which  $Fr_0 = 1/2$  for energy-conserving gravity currents. If the ambient is strongly stratified such that the ambient density at the bottom of the gate nearly equals the lock fluid density, then  $S \sim 1$  and, according to the definitions (2.4)–(2.6), we expect  $Fr_S \simeq Fr_1 \sqrt{S}$ , in which  $Fr_1 = 1/4$ .

In the following we adapt these results to currents flowing downslope. First, we assume that the slope is small so that the effects of the slope on the front speed may be ignored (Britter & Linden 1980). Second, we assume that the downslope speed,  $U$ , is constant up to the point of separation from the slope. The experimental results in §5.1 verify this assumption.

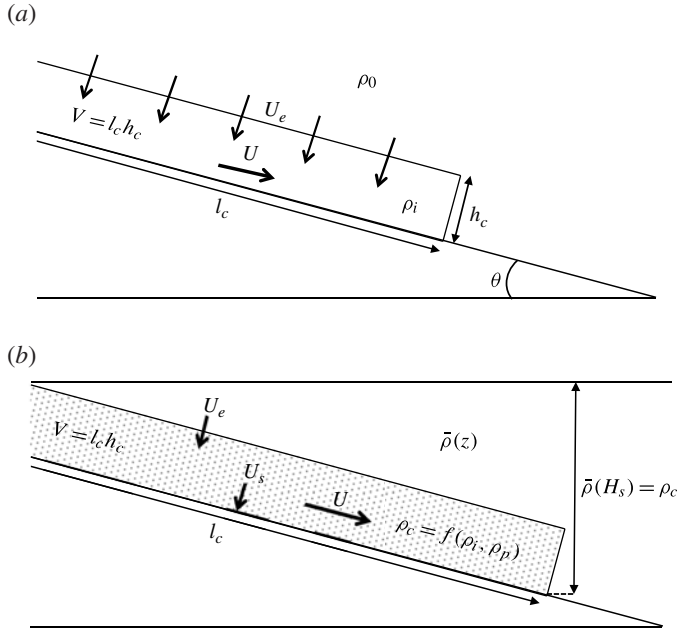


FIGURE 1. Box model description for (a) the evolution of interstitial fluid as it flows down the slope and entrains fluid from the stratified ambient with entrainment speed  $U_e = EU$  and (b) the combined effect of the interstitial fluid entrainment and particle settling illustrating that the current separates at  $z = H_s$ , where the current density,  $\rho_c$ , equals the density,  $\bar{\rho}(H_s)$ , of the stratified ambient. Although the current originates from a finite-length lock of volume  $V_0$ , entrainment is assumed to maintain a constant height of the current along its length, consistent with observations of experiments.

### 2.2. Entrainment, particle settling and separation depth

The separation depth is determined by factors that affect the density of the current as it propagates down the slope, including the entrainment of the ambient into the interstitial fluid and the settling of the particles. These factors are considered separately as represented in figure 1. Their effects are then combined to formulate a prediction for the separation depth.

The specific formulation of the box model we use is inspired by the observed structure of downslope gravity currents in our experiments, as shown in §4.1. While a particle-free current released from a finite-length lock into a uniform-density ambient has a well-defined turbulently entraining head with a thin tail behind, as observed in the constant-volume-flux experiments of Britter & Linden (1980), we find that turbulent entrainment extends well behind the head when the current propagates downslope in a stratified ambient. For particle-laden currents, sedimentation increases the buoyancy of the current, which further acts to bulk up the tail behind the head. Rather than estimate the length of the mixing region, we minimize the number of free parameters in the box model by fixing the height of the gravity current between the head and point of release. Thus, unlike the box model used by Hallworth *et al.* (1996) in their examination of bottom-propagating currents released from a finite-length lock, the volume of current in our model increases as it flows downslope and entrains ambient stratified fluid.

### 2.2.1. Entrainment into interstitial fluid

The infinitesimal change in interstitial density,  $d\rho_i$ , resulting from entrainment of ambient fluid of density  $\rho_0$  changing the volume per width by  $dV$  is given by  $d\rho_i = (\rho_0 - \rho_i) dV/V$ . Assuming  $\rho_0$  is constant, this is integrated to give a formula relating the interstitial fluid density,  $\rho_i$ , to the current volume,  $V$ :

$$\rho_i = \rho_0 - \frac{V}{V_0}(\rho_0 - \rho_{i0}), \quad (2.7)$$

where  $\rho_{i0}$  and  $V_0$  are the initial interstitial density and volume, respectively, of the fluid in the lock.

The volume itself is assumed to change as a result of entrainment of the ambient fluid into the current, a process that is assumed to be independent of particle concentration and settling. Entrainment processes are approximated by a two-dimensional box model, which neglects across-slope motion. Entrainment is assumed to depend upon the speed of the flow such that the ratio,  $E$ , of the entrainment speed  $U_e$  to current speed  $U$  is constant. For currents on a flat bottom, the entrainment has been observed to occur within the head of the flow with entrainment constant  $E = 0.063 \pm 0.003$  (Hallworth *et al.* 1996). However, for flow on relatively shallow slopes, the value of  $E$  is expected to depend upon the magnitude of the slope (Britter & Linden 1980; Beghin *et al.* 1981; Hallworth *et al.* 1996; Hughes & Griffiths 2006). The presence of ambient stratification is also expected to influence the magnitude and spatial distribution of entrainment. In particular, our experiments suggest that entrainment takes place far downstream of the current head. For simplicity, we assume that the current has uniform height  $h_c$  along its length  $l_c$ , as shown in figure 1(a). How we determine  $E$  for comparing theory with turbidity current experiments is described in § 5.2.

Hence, the change in volume per unit width occurring over infinitesimal time  $dt$  is given by

$$dV = U_e l_c dt = E U l_c dt, \quad (2.8)$$

in which  $V \equiv h_c l_c$ . If the current is released from a lock of length  $l_0$  and we assume that it immediately has constant speed  $U$ , then the length of the current increases linearly in time according to  $l_c = l_0 + Ut$ . Putting this in (2.8), integrating, writing the result in terms of  $l_c$  rather than  $t$  and recasting this in terms of the current depth  $H_c = sl_c$  through the slope  $s$  gives

$$\frac{V}{V_0} = 1 + \frac{E}{2s} \left[ \left( \frac{H_c}{h_0} \right)^2 - 1 \right]. \quad (2.9)$$

Here we have used  $h_0 = sl_0$  to relate the height of the lock fluid at the gate to its initial length and we have used the fact that the lock is triangular to write its initial volume per width as  $V_0 \equiv h_0 l_0 / 2 = s l_0^2 / 2$ .

The result (2.9) can be used in (2.7) to predict the interstitial fluid density as a function of the depth  $H_c$  of the current front. In deriving (2.7), we have assumed that the ambient density  $\rho_0$  is uniform. For a gravity current propagating downslope in a stratified ambient, we may take (2.7) as a good approximation if the ambient density does not vary significantly from a characteristic value  $\rho_0$  over the depth of propagation of the current.

### 2.2.2. Particle settling

The turbidity current density decreases not only due to ambient entrainment, but also due to particle settling. In the experiments reported upon here, the particles are

glass spheres, which do not flocculate within the current. Suitably low concentrations of the particles (volume fractions  $< 0.15$ ) are used so no hindered settling of the particles is expected. Particle resuspension is ignored.

The concentration of the particles within the current is assumed to change due to particle settling at a speed  $U_s$ , as indicated in figure 1(b). The range of particle sizes varies in a particular experiment by a small amount (e.g.  $d = 38\text{--}53\ \mu\text{m}$ ) so that  $U_s$  is assumed to be approximately constant. If the particles are sufficiently small,  $U_s$  is given by the Stokes settling speed

$$U_s \simeq \frac{gd_p^2(\rho_p - \rho_0)}{18\rho_0\nu}, \quad (2.10)$$

where  $\nu$  is the kinematic viscosity ( $\nu = 10^{-6}\ \text{m}^2\ \text{s}^{-1}$  for fresh water),  $d_p$  is the diameter of the particles and it is assumed that the particle density,  $\rho_p$ , is so much greater than the interstitial fluid density that one can approximate  $\rho_i \simeq \rho_0$ .

We assume that the flow is sufficiently turbulent that the particles are uniformly mixed within the current of depth  $h_c$ , with mass loss taking place only due to settling at the lower boundary of the current (Martin & Nokes 1989; Bonnetcaze *et al.* 1993; Huppert 2006). Therefore, the change in time of the total mass of the particles in the current is

$$dm_p = -\frac{m_p}{h_c}U_s dt. \quad (2.11)$$

Combining (2.11) with (2.8) to eliminate  $dt$ , using  $V = h_c l_c$  and integrating gives an equation relating the total particle mass,  $m_p$ , to the current volume per unit width:

$$m_p = m_{p0} \left( \frac{V}{V_0} \right)^{-\gamma}, \quad (2.12)$$

in which  $m_{p0}$  is the mass of particles in the lock. Here we have defined the parameter  $\gamma$  to be the ratio of the particle settling speed to the entrainment speed:

$$\gamma \equiv \frac{U_s}{U_e}. \quad (2.13)$$

According to (2.12), there is little change in the particle mass if the settling speed is relatively small, but particles are depleted quickly if they settle faster than fluid is entrained into the current.

From the expression (2.12) for particle mass, we can relate the volume fraction of particles,  $\phi = m_p/(\rho_p V)$ , to the volume of the current:

$$\phi = \phi_0 \left( \frac{V}{V_0} \right)^{-\gamma-1}, \quad (2.14)$$

in which  $\phi_0$  is the volume fraction of particles in the lock.

Hence, the total density of the turbidity current is

$$\rho_c = \rho_i + \phi(\rho_p - \rho_i), \quad (2.15)$$

in which  $\rho_i$  and  $\phi$  are functions of the current volume through (2.7) and (2.14), respectively.

### 2.2.3. Separation depth

The current is assumed to separate from the slope and intrude into the stratified ambient at a depth  $H_s$  when its density,  $\rho_c$ , equals the density of the ambient at the

front position,  $\rho_s \equiv \bar{\rho}(H_s)$ , as illustrated in figure 1(b). In terms of the density at the top and bottom of the ambient of total depth  $H$ ,

$$\rho_s = \rho_0 + (\rho_B - \rho_0) \frac{H_s}{H}. \quad (2.16)$$

Equating (2.16) and (2.15) and using (2.7) and (2.14) gives an equation relating the separation depth  $H_s$  to the volume,  $V_s$ , of the current when it reaches this depth. The problem is closed using (2.9), which relates the current volume to depth through entrainment. The result is simplified, however, if we assume that the particle density is so much larger than the ambient or interstitial fluid density that we can approximate  $\rho_p - \rho_i \simeq \rho_p - \rho_0$  on the right-hand side of (2.15). Likewise, assuming that  $\rho_i - \rho_0$  is negligible compared with density difference due to particles, we have

$$\left[ 1 + \frac{E}{2s} \left( \frac{H_s^2}{h_0^2} - 1 \right) \right]^{-\gamma-1} = S \frac{H_s}{h_0}, \quad (2.17)$$

in which we have used  $\phi_0(\rho_p - \rho_0) \simeq \rho_{c0} - \rho_{h0}$  and the definition (2.6) to cast the background density gradient in terms of the stratification parameter,  $S$ .

Equation (2.17) implicitly defines the relative separation depth,  $H_s/h_0$ , as it depends upon entrainment  $E$ , slope  $s$ , relative stratification  $S$  and relative particle settling speed  $\gamma$ . We may use this to find explicit approximate expressions for the separation depth in the limits of long and short relative descent.

*Case 1 (long descent):*  $H_s^2/h_0^2 - 1 \gg 2s/E$

In this case the left-hand side of (2.17) is approximately  $[(E/s)(H_s/h_0)^2]^{-\gamma-1}$ . Hence, solving for  $H_s/h_0$  gives

$$\frac{\Delta H_s}{h_0} = \left[ \left( \frac{2s}{E} \right)^{\gamma+1} \frac{1}{S} \right]^{1/(2\gamma+3)}, \quad (2.18)$$

where the descent depth is defined to be the difference between the separation depth and the initial lock depth such that  $\Delta H_s = H_s - h_0$ . Putting this result back into the limiting condition for this case, the downslope descent is expected to be long if the relative stratification is sufficiently weak:  $S \ll (E/2s)^{1/2}$ .

*Case 2 (short descent):*  $(H_s^2/h_0^2) - 1 \ll 2s/E$

In this case the left-hand side of (2.17) is approximately unity, and so the relative separation depth is

$$\frac{\Delta H_s}{h_0} = \frac{1}{S}. \quad (2.19)$$

This result depends only upon the stratification parameter,  $S \equiv (\rho_{h0} - \rho_0)/(\rho_{c0} - \rho_0)$ , and amounts to the condition that the flow separates at the ambient fluid depth where the density there matches the initial lock density. That is to say, the flow separates so close to the lock that entrainment and settling play no important role in changing the current density before it separates. The influence of entrainment and slope implicitly enter into the result (2.19) through the asymptotic constraint that  $S \gg (E/2s)^{1/2}$ .

The asymptotic analyses show that the transition from long to short descent occurs where  $S \sim (E/2s)^{1/2}$ , in which case

$$\frac{\Delta H_s^*}{h_0} \sim \frac{1}{S} \sim \sqrt{\frac{2s}{E}}. \quad (2.20)$$



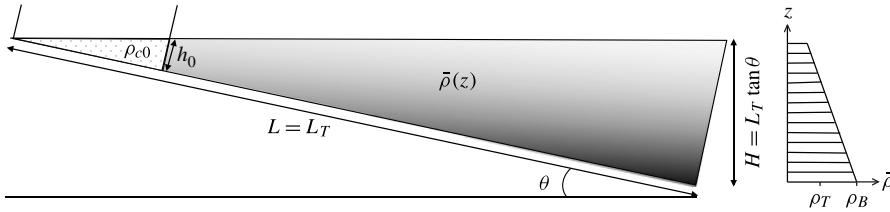


FIGURE 2. Schematic of the experimental set-up showing the ambient linear stratification (right and gradient grey-scale). The lock fluid behind the gate of height  $h_0$  has density  $\rho_{c0}$  set through a combination of the interstitial fluid density and particle concentration.

### 2.3. Particle concentration at separation depth

In many biological and industrial applications, it is useful to know the quantity of particles in a turbidity current that settle out along the slope and the amount that continue to be transported into the ambient by the intrusion (Cortés *et al.* 2014). In particular, the particle concentration in the current when it reaches the separation depth is given by combining (2.14) with (2.9) evaluated at  $H_c = H_s$ :

$$\begin{aligned} \phi_s &= \phi_0 \left[ 1 + \frac{E}{2s} \left( \frac{H_s^2}{h_0^2} - 1 \right) \right]^{-\gamma-1} \\ &= \begin{cases} \phi_0, & S \gg (E/2s)^{1/2}, \\ \phi_0 \left[ \left( \frac{E}{2s} \right)^{\gamma+2} \frac{1}{S} \right]^{-1/[(\gamma+1)(2\gamma+3)]}, & S \ll (E/2s)^{1/2}. \end{cases} \end{aligned} \quad (2.21)$$

If we assume that there is no entrainment into the current after it intrudes into the ambient, then the only change in intrusion density is due to the settling of the particles. From (2.11), the resulting particle concentration decreases after the separation time,  $t_s$ , according to

$$\phi = \phi_s e^{-(U_s/h_{cs})(t-t_s)}, \quad (2.22)$$

in which the current height at the separation point,  $h_{cs}$ , is assumed to be constant.

## 3. Experimental set-up

Lock exchange experiments were conducted in a rectangular tank of width  $W = 4.5$  cm, length  $L_T = 120.8$  cm and height  $H_T = 18.5$  cm, as shown in figure 2. The tank was raised at one end to produce the sloping bottom. Two slope angles were considered,  $\theta = 8.4^\circ$  and  $\theta = 4.4^\circ$ , corresponding to slopes of  $s = 0.148$  and  $0.077$ , respectively. The former case corresponds to  $\theta = \tan^{-1}(H_T/L_T)$ , which is the largest possible angle allowing fluid in the tank to span the entire length,  $L_T$ .

The standard ‘double-bucket’ method was modified to fill the tank to depth  $H = L_T \tan \theta$  with uniformly stratified ambient. In this method, the volume of the salt water bucket was half that of the fresh water bucket. Thus, as fluid was extracted from the salt water bucket and fresh water displaced into it, the density in this bucket decreased quadratically in time. Because the vertical cross-section of the tank was triangular, the resulting ambient density decreased linearly with height from the bottom corner. After filling, samples were taken by a syringe at 5 cm vertical

intervals in experiments with  $\theta = 8.4^\circ$  and at 3 cm vertical intervals in experiments with  $\theta = 4.4^\circ$ . The densities of the samples were measured by an Anton Paar DMA 58 density meter with an accuracy of  $10^{-4} \text{ g cm}^{-3}$ . This confirmed that the density as a function of height was linear. The buoyancy frequency,  $N$ , was determined by finding the slope of the best-fitting line through plots of the measured density versus height. Experiments were conducted with uniform-density ambients ( $N = 0$ ) and with strong ambient stratification as characterized by  $N = 0, 1.12, 1.9$  and  $3.0 \text{ s}^{-1}$ , with the surface density ranging from  $\rho_T = 0.998$  to  $1.02 \text{ g cm}^{-3}$  and the bottom density ranging from  $\rho_B = 0.998$  to  $1.20 \text{ g cm}^{-3}$ .

An acrylic gate edged with a foam seal was inserted at the shallow end of the tank to produce the lock. The length and height of the lock were varied by changing the along-slope position of the gate from the shallow end of the tank. Lock heights of  $h_0 = 3, 4.5$  and  $6 \text{ cm}$  were considered.

The ambient fluid was established with the gate in place. To inhibit the exchange of fluid past the gate, fluid was added to the lock during the last stages of filling the tank so as to keep the surface approximately level on either side of the gate.

Some experiments were performed with no particles and uniform-density saline fluid in the lock, with salt water densities ranging from  $\rho_{S0} = 1.005$  to  $1.16 \text{ g cm}^{-3}$ . In experiments with particles, the lock fluid was fresh water with the interstitial density,  $\rho_{i0} = 0.998 \text{ g cm}^{-3}$ . The particles were glass spheres (MO-SCI Corporation) of density  $\rho_p = 2.5 \text{ g cm}^{-3}$ . Five different types of particle batches were used, each batch having a range of diameters  $d_p$  about a mean value  $\bar{d}_p$ . Explicitly, the particles are characterized by  $\bar{d}_p = 20 \text{ }\mu\text{m}$  ( $1 < d_p < 38 \text{ }\mu\text{m}$ ),  $\bar{d}_p = 29 \text{ }\mu\text{m}$  ( $13 < d_p < 45 \text{ }\mu\text{m}$ ),  $\bar{d}_p = 46 \text{ }\mu\text{m}$  ( $38 < d_p < 53 \text{ }\mu\text{m}$ ),  $\bar{d}_p = 64 \text{ }\mu\text{m}$  ( $53 < d_p < 75 \text{ }\mu\text{m}$ ) and  $\bar{d}_p = 76 \text{ }\mu\text{m}$  ( $63 < d_p < 90 \text{ }\mu\text{m}$ ). The composite density of the particle-laden fluid within the lock,  $\rho_{c0}$ , was then determined by the mass of particles added to the given volume of fresh water within the lock. The volume fraction of added particles was always smaller than  $\phi_0 = 0.15$ , so that the change in lock volume due to addition of particles was considered negligible. In turbidity current experiments  $\rho_{c0}$  ranged from  $1.02$  to  $1.21 \text{ g cm}^{-3}$ . In all cases, a small amount of food colouring was added to the lock fluid. In turbidity current experiments, the lock fluid was vigorously mixed to ensure the particles were uniformly distributed. The gate was vertically extracted a short time after this mixing stopped.

In typical experiments where intrusion occurred, the lock fluid ran downslope at speeds,  $U$ , ranging from  $0.02$  to  $0.2 \text{ m s}^{-1}$ . The corresponding Reynolds number based on the lock height was of the order of  $Re \equiv Uh_0/\nu \sim 3000$ , in which we have used the kinematic viscosity for fresh water,  $\nu \simeq 10^{-6} \text{ m}^2 \text{ s}^{-1}$ . As a consequence, we expect viscosity to have negligible effect upon bottom friction and turbulent entrainment.

A digital camera recorded the flow of the current at 24 frames per second with a spatial resolution of approximately  $8 \text{ pixels cm}^{-1}$ . The camera was placed  $2 \text{ m}$  from the tank, perpendicular to the centre of the tank and at the height of the fluid surface. Supplementary movies are available at <http://dx.doi.org/10.1017/jfm.2014.413>. The movies were analysed using MATLAB. In particular, the measured current speed,  $U$ , and separation depth,  $h_s$ , were determined by constructing along-slope time series. From each snapshot from the movie, the pixels along a line parallel to the slope and moderately ( $\sim 0.5 \text{ cm}$ ) above it were extracted and sequentially stacked in time. From the resulting image, the advance and halting of the current front were easily identified.

An example of the progression of downslope flow is shown in figure 3. This shows snapshots from a typical turbidity current experiment at times shortly after the

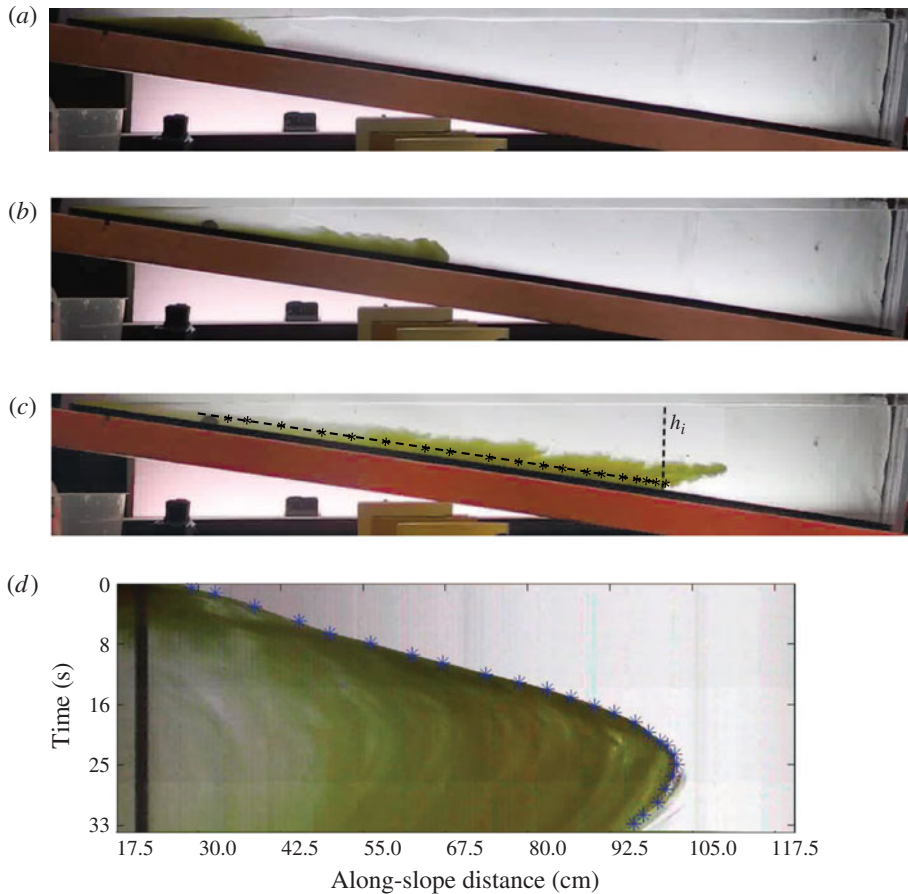


FIGURE 3. (Colour online) Snapshots from a turbidity current experiment: (a) after gate extraction at  $t = 1$  s; (b) turbidity current set up at  $t = 10$  s; (c) current separated from slope and intrudes at  $t = 26$  s. (d) Along-slope time series constructed by stacking slices through successive snapshots with the slices parallel to and 0.5 cm above the slope. The separation depth is indicated in panel (c), and selected locations of the front position versus time are indicated by the stars in panel (d) and compared with the stars in panel (c). In this experiment  $s = 0.148$ ,  $N = 1.1 \text{ s}^{-1}$ ,  $h_0 = 3.3 \text{ cm}$ ,  $\rho_{c0} = 1.02 \text{ g cm}^{-3}$  and  $\bar{d}_p = 20 \text{ }\mu\text{m}$ . (See supplementary movie 1.)

gate has been extracted (figure 3a), after it is well developed and flows downslope at near-constant speed (figure 3b) and shortly after it has separated from the slope and intrudes into the stratified ambient (figure 3c). The measured separation depth is indicated in figure 3(c). However, it is the along-slope time series shown in figure 3(d) that is used to measure both  $U$  and  $h_s$ . The along-slope position of the front versus time is determined by locating a sequence of points at the interface between the dyed current and clear ambient (illustrated by the stars in figure 3d). The current speed is determined as the slope of the best-fitting line through the points between the time of release and shortly before the current separates from the slope. After locating the maximum along-slope propagation distance,  $l_s$ , the separation depth is determined as  $h_s = sl_s$ , in which  $s = \tan \theta$  is the bottom slope.

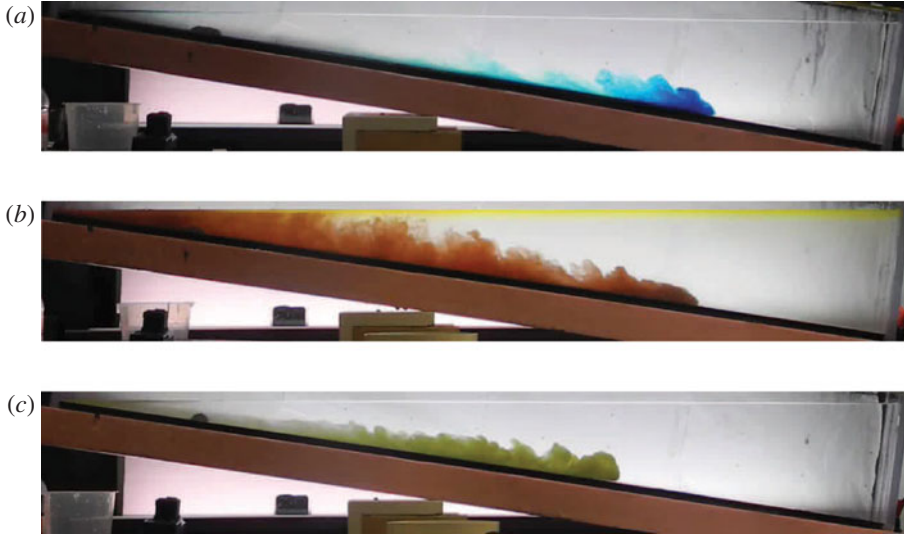


FIGURE 4. (Colour online) Snapshots from three different experiments all with slope  $s = 0.147$  and lock height  $h_0 = 3$  cm: (a) saline gravity current,  $N = 0$  ( $\rho_{i0} = \rho_{c0} = 1.015$  g cm $^{-3}$ ) in a uniform ambient ( $\rho_0 = 0.998$  g cm $^{-3}$ ); (b) turbidity current,  $N = 0$  ( $\bar{d}_p = 20$   $\mu$ m,  $\rho_{i0} = 0.998$  g cm $^{-3}$  and  $\rho_{c0} = 1.2$  g cm $^{-3}$ ) in a uniform ambient ( $\rho_0 = 1.07$  g cm $^{-3}$ ); and (c) turbidity current,  $N = 1.1$  s $^{-1}$  ( $\bar{d}_p = 20$   $\mu$ m,  $\rho_{i0} = 0.998$  g cm $^{-3}$  and  $\rho_{c0} = 1.02$  g cm $^{-3}$ ) in a uniformly stratified ambient. The last case corresponds to the same experiment shown in figure 3 with the snapshot shown at a time between figure 3(b,c) when the turbidity is at the point of separating from the slope and intruding into the ambient. (See supplementary movies: movie 1 and 2: fig 4a; movie 3: fig 4b.)

The main limitation of this experimental set-up is the limited size of the tank. While we were able to explore a suitable parameter space for all the defining quantities of our theory, a larger tank would have allowed a wider range of parameter results, as the certain stratifications and densities led to the turbidity or gravity current reaching the end of the tank before intrusion. Such cases obviously could not then be applied to our theory. The tank size also limited the range of slopes that could be applied in the experiments. The experimental set-up was not designed to measure the quantity of sediment deposition along the bottom of the tank. So we were unable to test the predictions given in § 2.3 for along-slope particle concentration.

## 4. Qualitative results

### 4.1. Along-slope evolution: gravity and turbidity currents

Figure 4 compares the structure of saline and particle-laden gravity currents in a uniform-density ambient as well as comparing the structure of turbidity currents in unstratified and stratified fluid. Consistent with the large Reynolds numbers of all our experiments, in all three cases the currents exhibit significant turbulence in the head and in the lee of the current. As in the low-slope experiments of Britter & Linden (1980) and Beghin *et al.* (1981), the saline gravity current propagates downslope with the dense fluid concentrated at the head and relatively little saline fluid suspended in the ambient in the far lee (figure 4a).



FIGURE 5. (Colour online) A snapshot from the same experiment shown in figures 3 and 4(c) but taken at a time well after the current has separated from the slope. Several fingers of dye are evident emanating horizontally into the stratified ambient along the length of the slope.

In contrast, as a turbidity current of fresh water mixed with particles runs downslope into a uniform-density saline ambient, a significant amount of fluid originating from the lock remains suspended in the ambient well behind the current front (figure 4b). This occurs because, as particles settle out along the current length, the composite density decreases until the particle concentration is so small that the (upward) buoyancy of the interstitial fluid overcomes the (downward) buoyancy associated with the particles. Over time the particles rain out altogether and the interstitial fluid rises and propagates along the surface.

The structure in the lee of a turbidity current is different still when it propagates downslope into a stratified ambient (figure 4c). In this case, the tail of the turbidity current more closely resembles that of the saline gravity current in a uniform-density ambient. Even though particles settle out, the interstitial fluid mixes with the stratified ambient so that its density becomes so great that it is no longer buoyant compared to the surface waters. Indeed, as the turbidity current descends, the interstitial fluid becomes increasingly dense until the combination of reduced particle concentration and higher interstitial density gives a composite density comparable to the ambient density at the current front. The snapshot shown in figure 4(c) is shown just at the point of separation of the current from the slope, with the structure at later and earlier times shown in figure 3.

These observations of the long extent of turbulent mixing behind the head of turbidity currents in a stratified ambient help justify the box-model approximation in § 2.2, whereby the height of the current is assumed constant along its length.

#### 4.2. Separation in stratified ambients: intrusions and fingering

After the turbidity current separated from the slope and intruded into the ambient, turbulence was suppressed around the head of the intrusion but particle settling continued to occur. In most experiments, the density change resulting from particle loss did not significantly impact the depth of the intruding fluid. The intrusion was observed to advance horizontally at a much slower speed, becoming narrower as the intrusion spread along the depth of neutral buoyancy.

In experiments of both turbidity and gravity currents in stratified ambients, even as the current nose separated from the slope and intruded into the ambient, the interstitial fluid along the tail of the current also detrained into the ambient, forming a series of smaller intrusions, or ‘fingers’. These are apparent in figure 5, which shows a snapshot of the same experiment shown in figures 3 and 4(c) but long after at a time when the system settled down and became stationary. Above the lowest intrusion, fingers of dye originating from the lock fluid clearly emanated from the slope horizontally into the ambient.

Similar fingering phenomena have been found previously as a double outflow observed for a gravity current flowing downslope into a linearly stratified ambient (Baines 2008). The fingering also occurred when a gravity current was continuously discharged down an incline into uniform stratification while the inflowing density changed linearly with time (Fernandez & Imberger 2008). The vertical scale of this fingering depended upon downslope speed,  $U$ , with larger velocities providing larger spacing between fingers. In our experiments, there was no clear trend relating the measured distance between fingers to characteristic length scales based upon  $U/N$  or  $U\sqrt{h_0/g_0}$ . In turbidity current experiments, this may be because another effect plays a role, that of lofting of relatively light interstitial fluid as particles settle out.

While fingering is of some theoretical interest, understanding the formation and structure of fingers would require experiments with finer particles performed in longer tanks so that endwall effects would be unimportant during the time of formation of the fingers. Such an examination lies beyond the focus of this paper and so we do not speculate further as to the primary mechanisms defining this effect.

#### 4.3. Excitation and influence of internal waves

The along-slope time series in figure 3(d) shows that the turbidity current moves downslope at near-constant speed almost instantly after release from the lock, and it slows to a halt over a relatively small distance before separating from the slope and intruding into the stratified ambient. The time series also shows that the front of dyed fluid on the slope moves back upslope after reaching its separation depth. This is a consequence of internal waves that are generated in the tank by the downslope current.

This assertion is demonstrated in figure 6, which shows the along-slope position of the front as a function of time measured from three experiments. In all three cases, the current propagates at nearly constant speed shortly after release from the lock and then rapidly decelerates to a halt at the separation depth. This occurs around non-dimensional time  $Nt = 18$  in all three cases, although one should not expect this to be a universal result. The along-slope distance at which separation occurs increases from  $l_s = 40$  to 60 to 90 cm as the lock density increases from  $\rho_{c0} = 1.02$  to 1.1 to 1.2 g cm<sup>-3</sup>, respectively. Thereafter, the front position moves back upslope and does so to a greater degree as  $\rho_{c0}$  (and consequently  $l_c$ ) increases. The ensuing upslope and downslope motion oscillates with the frequency and amplitude increasing as  $l_c$  increases. These oscillations are attributed to internal waves generated by the turbidity current and consequent intrusions.

Further evidence for the existence and structure of internal waves is shown in figure 7. In this experiment a turbidity current separates from the slope a short distance from the lock. A vertical dye line, formed by dropping potassium permanganate crystals before the start of an experiment, remains vertical even as the intrusion progresses horizontally away from the slope (figure 7a). Later the front of the intrusion stops advancing, but the vertical dye line is observed to displace rightwards and leftwards with approximately two-and-a-half undulations across its depth with vertically varying wavelength (figure 7b). These undulations are not stationary, but continue to move back and forth in time. After  $t = 123$  s (figure 7d), there are approximately four undulations over the depth at the location of the dye.

From many experiments in which a vertical dye line was established, we found that the amplitude of the oscillations depended upon the initial density and speed of the downslope current, with larger slope speed producing larger-amplitude internal waves.

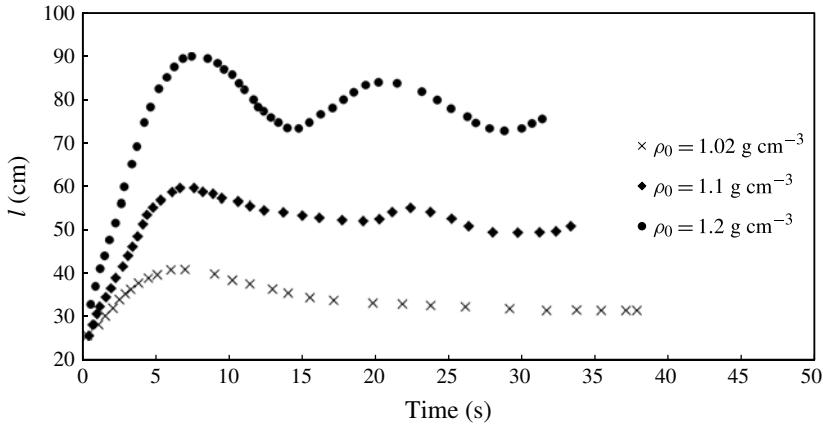


FIGURE 6. Along-slope position versus time determined from three experiments of turbidity currents with (composite) lock densities  $\rho_{c0} = 1.02 \text{ g cm}^{-3}$  (cross),  $1.1 \text{ g cm}^{-3}$  (open diamond) and  $1.2 \text{ g cm}^{-3}$  (closed circle). In each case  $s = 0.147$ ,  $N = 3.0 \text{ s}^{-1}$ ,  $h_0 = 3 \text{ cm}$  and  $\bar{d}_p = 29 \text{ }\mu\text{m}$ .

At later times, these internal waves were observed to interact with the intrusion, and overlying intrusive fingers if they developed.

Although internal waves may affect the evolution of the front position on the slope after the current separates, because the internal waves are not significant until after separation occurs, they are not expected to play an important role in setting the downslope speed and separation depth.

#### 4.4. The evolution of hypopycnal plumes

Although outside the main focus of this work, we did perform a small number of experiments examining the evolution of hypopycnal (surface-propagating) particle-bearing currents in uniform-density and stratified ambients.

Consistent with Parson *et al.* (2001), we found that the particles in a hypopycnal current eventually convectively settled out in a uniform-density ambient. However, in the experiment shown in figure 8, more complicated dynamics ensued. Here the settling particles carried some of the (fresh water) interstitial fluid down with them (figure 8*b*). The mixture of particles and relatively fresh interstitial fluid then flowed downslope as a turbidity current (figure 8*c*). But, as in figure 4(*b*), the particles eventually settled out to such an extent that the buoyancy of the current reversed once again, with interstitial fluid convectively rising once more to the surface, carrying a small number of particles with it (figure 8*d*). Finally, a rightward flowing surface current developed once more (figure 8*e*).

These convective instabilities are observed to be greatly hindered in the case of a strongly stratified ambient (not shown), with most cases showing the settling of particles after intrusion to be at a rate approximately proportional to the settling speed (see e.g. figure 7). In the particle-bearing intrusion experiments of de Rooij (1999), convective instability was observed if the ambient was weakly stratified ( $N \lesssim 1 \text{ s}^{-1}$ ).

Further investigation of these dynamics lies beyond the focus of this paper. However, the qualitative results demonstrate the complex non-local dynamic response of particle-bearing and particle-laden flows in stratified ambient fluids.

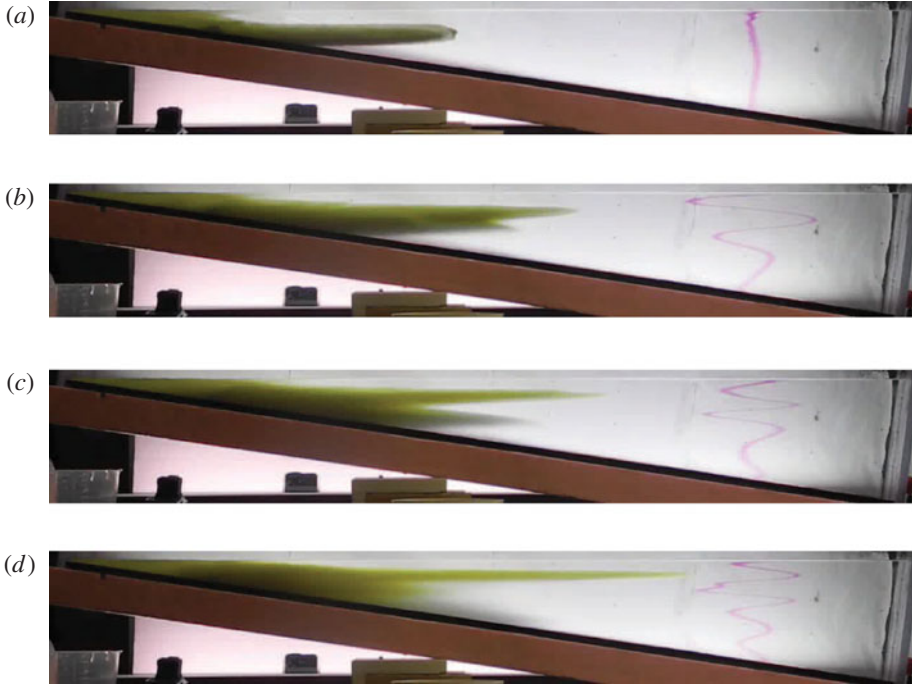


FIGURE 7. (Colour online) Evolution of a turbidity current with  $s = 0.147$ ,  $N = 1.9 \text{ s}^{-1}$ ,  $h_0 = 3 \text{ cm}$ ,  $\bar{d}_p = 20 \text{ }\mu\text{m}$  and  $\rho_{c0} = 1.12 \text{ g cm}^{-3}$  shown at various times: (a) 15 s, particle-filled intrusion; (b) 37 s, particles begin to settle; (c) 50 s, particles form layer within ambient; and (d) 123 s, particles on slope. The vertical dye line to the right shows the formation of horizontally long internal wave modes following the separation of the turbidity current from the slope and the consequent intrusion into the ambient. The horizontal tongue of dark fluid that descends over time between 37 and 123 s is a patch of particles that settles from the intrusion down to the underlying slope. (See supplementary movie 4.)

## 5. Quantitative results

### 5.1. Front velocity

From plots of along-slope front position versus time, as in figures 3(d) and 6, the steady-state current speed is determined from the slope of best-fitting lines through the plots determined over times shortly after release from the lock and before the current decelerates significantly as it approaches the separation depth. Figure 9 plots the measured relative front speed,  $u_s/\sqrt{g'_0 h_0}$ , against the relative stratification parameter,  $S$ , given by (2.6). The vertical error bars result mainly from errors in the estimate of  $g'_0$  reflecting the uncertainty in the mass of suspended particles. The results are compared with the predicted values of the Froude number  $Fr_S$  in the  $S \ll 1$  and  $S \sim 1$  limits.

In a uniform-density ambient ( $N = 0$ ), figure 9 shows that the non-dimensional front speed approaches a value of  $U/\sqrt{g'_0 h_0} = 1/2$ , consistent with the predicted Froude number for a steady current on a horizontal bottom in a constant-density ambient (Benjamin 1968; Shin *et al.* 2004; Ungarish 2006). In relatively weak ambient stratification, the non-dimensional frontal speed decreases, consistent with



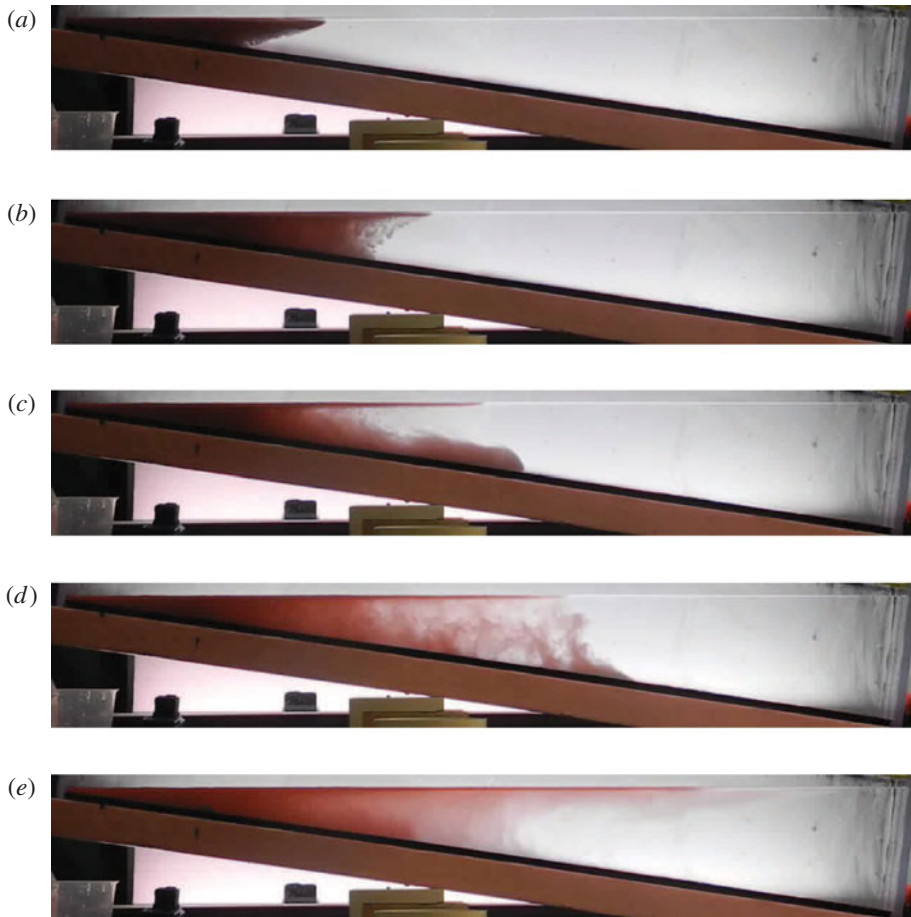


FIGURE 8. (Colour online) Evolution of a particle-bearing hypopycnal current in a uniform-density ambient where  $s=0.147$ ,  $h_0=3$  cm,  $\rho_0=1.07$  g cm $^{-3}$ ,  $\rho_{c0}=1.18$  g cm $^{-3}$  and  $\bar{d}_p=20$   $\mu$ m: (a)  $t=12$  s, after rapid particle settling an initial hypopycnal current develops shortly after the gate is extracted; (b)  $t=26$  s, convectively unstable falling particles result in particle settling; (c)  $t=49$  s, a turbidity current develops on the bottom slope; (d)  $t=112$  s, convectively unstable rising interstitial fluid develops after more particles settle out; and (e)  $t=149$  s, redevelopment of the hypopycnal current after interstitial fluid gathers at the surface. (See supplementary movie 5.)

the asymptotic prediction of  $Fr_S$  for small  $S$ . In relatively stronger stratification such that  $S \rightarrow 1$ , theory predicts that  $Fr_S$  increases to  $1/4$  (Maxworthy *et al.* 2002; Ungarish 2006). The few experiments performed with  $S$  near unity are consistent with this prediction. Consideration of these two limits shows that the downslope speed is approximately equal to the speed of a gravity current on a horizontal bottom, consistent with Britter & Linden (1980). So we expect for the full range of stratification parameters,  $S$ , that the speed of the downslope gravity current is not influenced by the magnitude of the slope,  $s$ , at least for the relatively small slopes in our experiments. The speed shortly after release is set by the  $S$ -dependent Froude number defined through the conditions at the gate. Although the buoyancy force (and hence the local Froude number) decreases as the current runs downslope,

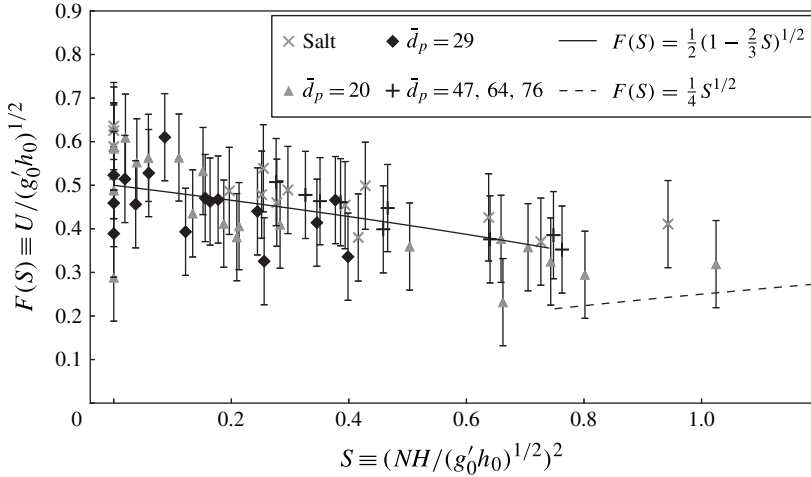


FIGURE 9. Non-dimensionalized front speed  $U$  versus the ratio of the effects of stratification  $N$  and initial buoyancy determined from the reduced gravity  $g'_0$ . ‘Salt’ refers to a saline gravity current with no particles (cross). The remaining cases are turbidity currents, which are initially composed of fresh water mixed with small particles of mean diameter  $\bar{d}_p = 20 \mu\text{m}$  (triangle), medium particles of mean diameter  $\bar{d}_p = 29 \mu\text{m}$  (square) and large particles of mean diameter one of  $\bar{d}_p = 46, 64$  or  $76 \mu\text{m}$ . Error bars are determined from measurement errors. The experimental results are then plotted with the theoretical values of  $F(S)$  for  $S \ll 1$  ( $Fr_S \simeq \frac{1}{2}(1 - \frac{2}{3}S)^{1/2}$ ) and  $S \sim 1$  ( $Fr_S \simeq \frac{1}{4}\sqrt{S}$ ) (Ungarish 2006).

apparently so does the opposing momentum force resulting from the entrainment of the stationary ambient fluid. Only when the current approaches the separation point does it decelerate as the buoyancy force decreases to zero and changes sign after the current overshoots its neutral buoyancy depth.

### 5.2. Separation depth

For currents that run sufficiently far downslope, the predicted intrusion depths depend upon the entrainment coefficient, which itself is expected to depend upon bottom slope (Britter & Linden 1980; Beghin *et al.* 1981; Hallworth *et al.* 1996), if sufficiently small. For experiments with a slope of  $s = 0.148$  ( $8.4^\circ$ ), we calibrate the value of  $E$  using measured values of the separation depth for (particle-free) saline gravity currents. From (2.18) with  $\gamma = 0$ , the descent depth is predicted to be  $\Delta H_s/h_0 = [2s/(ES)]^{1/3}$ . The predicted separation depth agrees best with the measured data using  $E = 0.05 (\pm 0.005)$ . For experiments with a slope of  $s = 0.077$  ( $4.4^\circ$ ), we choose  $E = 0.01$  consistent with that for saline gravity currents on  $5^\circ$  slopes (Turner 1973). Although the transition between the predicted depth for Cases 1 and 2 depends upon the value of the entrainment coefficient,  $E$ , the transition is relatively insensitive to the value of  $E$ . For example, according to (2.20), decreasing  $E$  from 0.08 to 0.04 changes the predicted relative transition depth by 14%.

The measured relative descent depth,  $\Delta h_s/h_0$ , for all experiments of bottom-propagating saline and turbidity currents that intrude into a stratified ambient is plotted against the theoretical value of  $\Delta H_s/h_0$  in figure 10.

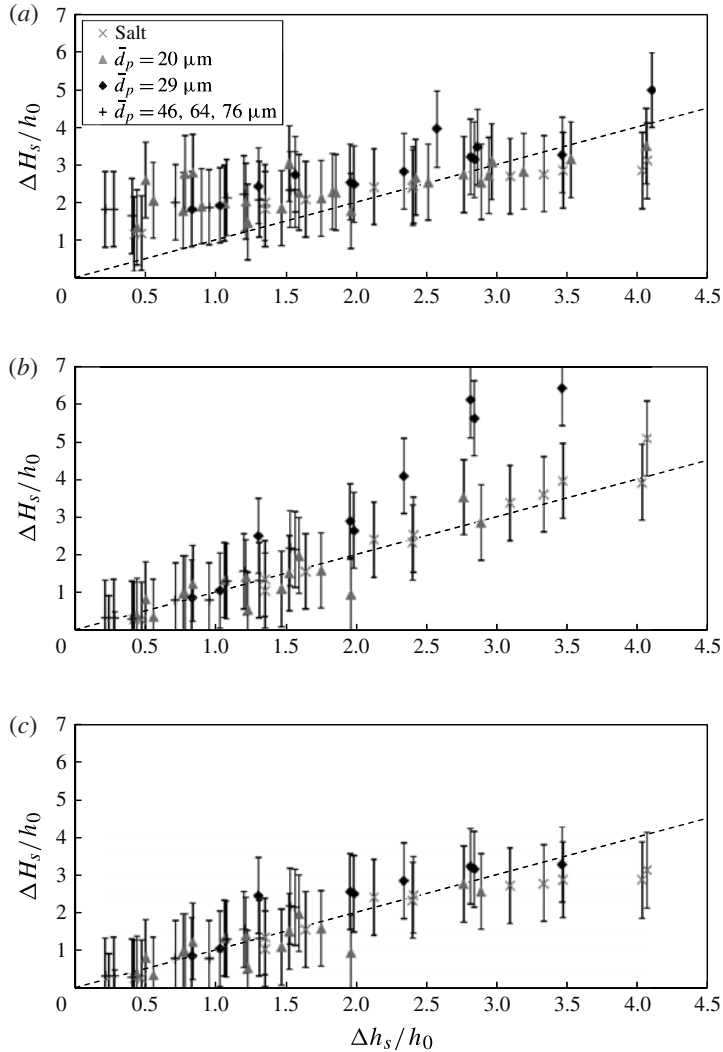


FIGURE 10. Predicted relative maximum descent of the current on the slope,  $\Delta H_s/h_0 \equiv (H_s - h_0)/h_0$ , plotted against the measured relative descent,  $\Delta h_s/h_0 \equiv (h_s - h_0)/h_0$ : (a) experiment versus long-propagation approximation (2.18) (Case 1); (b) experiment versus short-propagation approximation (2.19) (Case 2); and (c) experiment versus combined theory, a composite prediction where both cases are applied changing from Case 1 to Case 2 at the transition depth  $\Delta H_s^*$  given by (2.20). Different symbols are plotted depending upon the current composition as indicated in the legend. ‘Salt’ refers to a saline gravity current with no particles (cross). The remaining cases are turbidity currents, which are initially composed of fresh water mixed with small particles of mean diameter  $\bar{d}_p = 20 \mu\text{m}$  (triangle), medium particles of mean diameter  $\bar{d}_p = 29 \mu\text{m}$  (square) and large particles of mean diameter one of  $\bar{d}_p = 46, 64$  or  $76 \mu\text{m}$  (plus).

In figure 10(a), the measured values are compared with the long-propagation-distance prediction of Case 1 (2.18). This shows a linear trend for sufficiently large values of  $\Delta h_s/h_0 > \sqrt{2s/E} \approx 1.9$ .

Experiment	Mean difference		
	Case 1	Case 2	Combined
Salt	0.55	<b>0.26</b>	0.36
$\bar{d}_p = 20 \mu\text{m}$	0.73	0.33	<b>0.30</b>
$\bar{d}_p \geq 29 \mu\text{m}$	0.91	0.85	<b>0.32</b>
All experiments	0.76	0.51	<b>0.33</b>

TABLE 1. The mean value of  $|\Delta h_s - \Delta H_s|/h_0$  computed from the data shown in figure 10 using the theory with Case 1 or Case 2 alone and with the theory combining the two cases. The mean is computed separately using data for experiments with particle-free saline currents, experiments with small particles having mean diameter  $\bar{d}_p = 20 \mu\text{m}$ , experiments with medium and large particles ( $\bar{d}_p = 29, 46, 64$  or  $76 \mu\text{m}$ ), and for all experiments. The smallest mean values computed from each subset of experimental data are shown in bold.

In figure 10(b), the measured values are compared with the short-propagation-distance prediction of Case 2 (2.19). In this case, the medium to large particles deviate from the linear trend at larger values of  $\Delta h_s/h_0$ . Such a result is expected, as the approximation for Case 2 only applies when  $H_s < H_s^*$ , given by (2.20).

In figure 10(c) the experimental results are compared against the two asymptotic limits of the theory delimited by the critical separation depth given by (2.20). Explicitly,  $\Delta h_s/h_0$  is plotted against the prediction of (2.18) if  $S > \sqrt{E/2s}$  and  $\Delta h_s/h_0$  is plotted against the prediction of (2.19) if  $S < \sqrt{E/2s}$ .

We have performed various statistical analyses to demonstrate that the theory combining Cases 1 and 2 provides the closest fit to the measured  $\Delta h_s/h_0$ . Table 1 lists the mean relative discrepancy between observations and theory broken down in terms of particle size and the application of theory with Case 1 or 2 alone and the combined theory. The results show that the discrepancy is smallest in all turbidity current experiments using the combined theory. The greatest discrepancy when not allowing for the inclusion of  $\gamma$  occurs if the prediction of Case 2 is applied to experiments with particle sizes  $d_p \geq 29 \mu\text{m}$ .

We also calculated the  $p$ -values for the slope between the measured  $\Delta h_s/h_0$  and theoretical data  $\Delta H_s/h_0$  compared to the slope in a case where the slope is unity with a standard error of 0.5, based on estimates of the measured  $\Delta h_s/h_0$  error. These values verified that the trends were not statistically different from the hypothesis  $\Delta h_s/\Delta H_s = 1$  except when comparing the prediction of Case 2 to experimental measurements for moderately large particles with  $\bar{d}_p \geq 29 \mu\text{m}$ . Comparing the slopes of the best-fitting lines through measurement versus prediction data, we found that values lay within an error of unity except when comparing the prediction of Case 2 to experiments with moderately large particles, in which case the slope was  $2.12 \pm 0.9$ , and when comparing the prediction of Case 2 to all experiments, in which case the slope was  $1.4 \pm 0.3$ .

Only for the case of particle-free saline gravity currents does Case 2 provide a more accurate prediction of the intrusion depth. This may be expected, as the saline currents have no particle settling and so the inclusion of the  $\gamma$  parameter in this case is not expected to provide any improvement on intrusion depth. Also, for small particle turbidity currents ( $\bar{d}_p = 20 \mu\text{m}$ ), where the current properties are most similar to that of a saline gravity current, Case 2 and the combined theory case produce an almost equivalent match between the measurements and theory.

Consistently we find that the prediction of Case 2, which neglects entrainment and particle settling under the assumption that separation occurs near the lock, does not well represent the intrusion depth particularly for moderately large particles. Case 2 does provide a better prediction for saline gravity currents and a comparably good prediction for turbidity currents with particles so small that little settling occurs before separation. However, our results conclusively show that, in general, it is necessary to include the effects of particle settling and entrainment in order to formulate a reliable prediction of the separation depth of turbidity currents.

If a longer tank had been used and the flow permitted to travel over a longer distance, then the effect of settling would potentially play a more dominant role for turbidity currents with the smallest particles. But over the short distances allowed, the settling was too slow to have a large impact on the density of the current. Hence the flow of these currents could be described solely through the simple dimensional relation of (2.19). However, the deviation of the medium to large particle situations in figure 10(b) indicates the necessity of allowing for both Case 1 and Case 2 situations in defining the characteristics of the flow for the larger particle cases, and hence the importance of the  $\gamma$  parameter in defining particle-laden currents where the particles play a dominant role or large separation depth may occur.

## 6. Conclusion

Laboratory experiments were conducted to investigate the effects of both slope and stratification upon the speed and separation depth of particle-driven gravity currents. As saline and particle-laden currents propagate downslope, both the front and trailing billows separate from the slope, forming fingers that intrude into the stratified ambient. Strong stratification also hinders the production of convective instabilities produced by the settling of particles in hypopycnal plumes observed for a constant-density ambient.

The turbidity current is found to have a constant speed almost immediately after release from the lock. This measured speed agreed well with shallow-water theory predictions for horizontally propagating gravity currents in weak and strong stratification. A scaling analysis incorporating the entrainment of interstitial fluid and the settling of particles predicted the separation depth of a particle-laden current travelling down slope into a stratified ambient. The predictions were verified by experiments performed with varying particle sizes, stratifications, slopes and particle volume fractions. For hyperpycnal turbidity currents travelling far from the lock (for which  $S > \sqrt{2s/E}$ ), the relative separation depth depends upon the relative stratification, slope, entrainment and  $\gamma$ , which is the ratio of particle settling to entrainment speed. For very small particles, the current evolves similarly to a saline gravity current in which case  $\gamma = 0$ . For currents that do not travel far from the lock, the relative separation depth depends only upon the relative stratification.

This work provides a starting point to help assess the risk from submarine avalanches to structures built on the continental margins and a means to more completely determine turbidity intrusion depths in thermally stratified lakes. But much remains to be done. Future work will examine continuous particle releases and the influence of non-uniform stratification and bottom topography.

## Acknowledgements

The authors are grateful for the constructive reviews provided by the anonymous referees of this paper and for the technical assistance provided by A. Jensen. This work was made possible due to the National Science Foundation (Grant OCE-0824636)

and the Office of Naval Research (Grant N00014-09-1-0844) in their support of the 2013 WHOI Geophysical Fluid Dynamics Summer School, where much of the work presented here was undertaken.

### Supplementary movies

Supplementary movies are available at <http://dx.doi.org/10.1017/jfm.2014.413>.

### REFERENCES

- ANTENUCCI, J. P., GHADOUAMI, A., BURFORD, M. A. & ROMERO, J. R. 2005 The long-term effect of artificial destratification on phytoplankton species composition in a subtropical reservoir. *Freshwat. Biol.* **50**, 1081–1093.
- BAINES, P. G. 2001 Mixing in flows down gentle slopes into stratified environments. *J. Fluid Mech.* **443**, 237–270.
- BAINES, P. G. 2008 Mixing in flows down gentle slopes into stratified environments. *Atmos.-Ocean* **46**, 405–419.
- BEGHIN, P., HOPFINGER, E. J. & BRITTER, R. E. 1981 Gravitational convection from instantaneous sources on inclined boundaries. *J. Fluid Mech.* **107**, 407–422.
- BENJAMIN, T. B. 1968 Gravity currents and related phenomena. *J. Fluid Mech.* **31**, 209–248.
- BIRMAN, V. K., BATTANDIER, B. A., MEIBURG, E. & LINDEN, P. F. 2007 Lock-exchange flow in slope channels. *J. Fluid Mech.* **577**, 53–77.
- BONNECAZE, R. T., HUPPERT, H. E. & LISTER, J. R. 1993 Particle-driven gravity currents. *J. Fluid Mech.* **250**, 339–369.
- BONNECAZE, R. T. & LISTER, J. R. 1999 Particle-driven gravity currents down planar slopes. *J. Fluid Mech.* **390**, 75–91.
- BRITTER, R. E. & LINDEN, P. F. 1980 The motion of the front of a gravity current travelling down an incline. *J. Fluid Mech.* **99**, 531–543.
- BRUSCHI, R., BUGHI, S., SPINAZZÉ, M., TORSELLETTI, E. & VITALI, L. 2006 Impact of debris flows and turbidity currents on seafloor structures. *Norw. J. Geol.* **86**, 317–336.
- DE CESARE, G., BOILLAT, J. L. & SCHLEISS, A. J. 2006 Circulation in stratified lakes due to flood-induced turbidity currents. *J. Environ. Engng* **132**, 1508–1517.
- CHUNG, S. W. & GU, R. 1998 Two-dimensional simulations of contaminant currents in stratified reservoir. *J. Hydraul. Engng* **124**, 704–711.
- CORTÉS, A., FLEENOR, W. E., WELLS, M. G., DE VINCENTE, I. & RUEDA, F. J. 2014 Pathways of river water to the surface layers of stratified reservoirs. *Limnol. Oceanogr.* **59**, 233–250.
- FERNANDEZ, R. & IMBERGER, J. 2008 Time-varying underflow into a continuous stratification with bottom slope. *J. Hydraul. Engng* **134**, 1191–1198.
- HALLWORTH, M. A., HUPPERT, H. E., PHILLIPS, J. C. & SPARKS, R. S. J. 1996 Entrainment into two-dimensional and axisymmetric turbulent gravity currents. *J. Fluid Mech.* **308**, 289–311.
- HOGG, A. J., HUPPERT, H. E. & HALLWORTH, M. A. 1999 Reversing buoyancy of particle-driven gravity current. *Phys. Fluids* **11**, 2891–2900.
- HOGG, A. J., HUPPERT, H. E. & HALLWORTH, M. A. 2000 Particle-driven gravity currents: asymptotic and box model solutions. *Eur. J. Mech. (B/Fluids)* **19**, 139–165.
- HUGHES, G. O. & GRIFFITHS, R. W. 2006 A simple convective model of the global overturning circulation, including effects of entrainment into sinking regions. *Ocean Model.* **12**, 46–79.
- HUPPERT, H. E. 2006 Gravity currents: a personal perspective. *J. Fluid Mech.* **554**, 299–322.
- HURZELER, B. E., IVEY, G. N. & IMBERGER, J. 1995 Spreading model for a turbidity current with reversing buoyancy from a constant-volume release. *Mar. Freshwat. Res.* **46**, 393–408.
- LAWRENCE, A. A., MCCAFFREY, W. D. & TALLING, P. J. 2009 Special issue introduction: Sediment gravity flows – recent insights into their dynamic and stratified/composite nature. *Mar. Petrol. Geol.* **26**, 1897–1899.
- MARTIN, D. & NOKES, R. 1989 A fluid-dynamics study of crystal settling in convecting magmas. *J. Petrol.* **30**, 1471–1500.

- MASSON, D. G., ARZOLA, R. G., WYNN, R. B., HUNT, J. E. & WEAVER, P. P. E. 2011 Seismic triggering of landslides and turbidity currents offshore Portugal. *Geochem. Geophys. Geosyst.* **12**, Q12011.
- MAXWORTHY, T., LEILICH, J., SIMPSON, J. E. & MEIBURG, E. H. 2002 The propagation of a gravity current into a linearly stratified fluid. *J. Fluid Mech.* **453**, 371–394.
- MONAGHAN, J. J., CAS, R. A. F., KOS, A. M. & HALLWORTH, M. 1999 Gravity currents descending a ramp in a stratified tank. *J. Fluid Mech.* **379**, 39–69.
- MULDER, T. & SYVITSKI, J. P. M. 1995 Gravity currents descending a ramp in a stratified tank. *J. Geol.* **103**, 285–299.
- MULDER, T., SYVITSKI, J. P. M., MIGEON, S., FAUGERES, J. C. & SAVOYE, B. 2003 Marine hyperpycnal flows: initiation, behaviour and related deposits. A review. *Mar. Petrol. Geol.* **20**, 861–882.
- PARSON, J. P., BUSH, J. W. M. & SYVITSKI, J. P. M. 2001 Hyperpycnal plume formation from riverine outflows with small sediment concentration. *Sedimentology* **48**, 465–478.
- PAULL, C. K., USSLER, W. III, GREENE, H. G., KEATEN, R., MITTS, P. & BARRY, J. 2003 Caught in the act: the 20 December 2001 gravity flow event in Monterey Canyon. *Geo-Mar. Lett.* **22**, 227–232.
- RIMOLDI, B., ALEXANDER, J. & MORRIS, S. 1996 Experimental turbidity currents entering density stratified water: analogues for turbidites in Mediterranean hypersaline basins. *Sedimentology* **43**, 527–540.
- DE ROOIJ, F. 1999 Sedimenting particle-laden flows in confined geometries. PhD thesis, University of Cambridge.
- DE ROOIJ, F., LINDEN, P. F. & DALZIEL, S. B. 1999 Saline and particle-driven interfacial intrusions. *J. Fluid Mech.* **389**, 303–334.
- SHEPARD, F. P., MCLOUGHLIN, P. A., MARSHALL, N. F. & SULLIVAN, G. G. 2013 Current-meter recordings of low-speed turbidity currents. *Geology* **5**, 297–301.
- SHIN, J. O., DALZIEL, S. B. & LINDEN, P. F. 2004 Gravity currents produced by lock exchange. *J. Fluid Mech.* **521**, 1–34.
- SPARKS, R. S. J., BONNECAZE, R. T., HUPPERT, H. E., LISTER, J. R., HALLWORTH, M. A., MADER, H. & PHILLIPS, J. 1993 Sediment-laden gravity currents with reversing buoyancy. *Earth Planet. Sci. Lett.* **114**, 243–257.
- STRAUB, K. M. 2007 Quantifying turbidity current interaction with topography. PhD thesis, Massachusetts Institute of Technology.
- THOMSON, R. E., DAVIS, E. E., HEESEMANN, M. & VILLINGER, H. 2010 Observations of long-duration episodic bottom currents in the Middle America Trench: evidence for tidally initiated turbidity flows. *J. Geophys. Res.* **115**, C006166.
- TOKYAY, T. E. & GARCIA, M. H. 2014 Effect of initial excess density and discharge on constant flux gravity currents propagating on a slope. *Environ. Fluid Mech.* **14**, 409–429.
- TURNER, J. S. 1973 *Buoyancy Effects in Fluids*. Cambridge University Press.
- UNGARISH, M. 2006 On gravity currents in a linearly stratified ambient: a generalization of Benjamin's steady-state propagation results. *J. Fluid Mech.* **548**, 49–68.
- WELLS, M. & NADARAJAH, P. 2009 The intrusion depth of density currents flowing into stratified water bodies. *J. Phys. Oceanogr.* **39**, 1935–1947.